Targeting IRS-1/2 in uveal melanoma inhibits *in vitro* cell growth, survival and migration, and *in vivo* tumor growth.

Chandrani Chattopadhyay[1], Rajat Bhattacharya[3], Jason Roszik[1&2], Fatima S. Khan[1], Gabrielle A. Wells[4], Hugo Villanueva[4], Yong Qin[5], Rishav Bhattacharya[6], Sapna Patel[1] and Elizabeth A. Grimm[1]

Departments of [1]Melanoma Medical Oncology, [2]Genomic Medicine and [3]Surgical Oncology, The University of Texas MD Anderson Cancer Center, Houston, Texas-77030, USA;

[4]Patient Derived Xenograft and Advanced In Vivo Models Core, and Department of Otolaryngology – Head and Neck Surgery, Baylor College of Medicine, Houston, Texas-77030, USA;

[5]Department of Pharmaceutical Sciences, The University of Texas at El Paso, El Paso, Texas-79968, USA;

[6]College of Agriculture and Life Sciences, Texas A & M at College Station, College Station, Texas-77843, USA.

Corresponding Author:

Chandrani Chattopadhyay, Ph.D.

1515 Holcombe Blvd., Unit 362

Houston, TX 77030

Phone: 713-792-3719

Fax:713-793-3531

Email: cchattop@mdanderson.org

Abstract: Uveal melanoma (UM) originating in the eye and metastasizing to the liver is associated with poor prognosis and has only one approved therapeutic option. We hypothesized that liver-borne growth factors may contribute to UM growth. Therefore, we investigated the role of insulin-like growth factor -1 and its receptor (IGF-1/IGF-1R) signaling in UM. We found that the insulin receptor substrate -1 (IRS-1) is overexpressed in UM cells and tumors. Since we previously observed that IGF-1R antibody therapy was not clinically effective in UM, we investigated the potential of NT157, a small molecule inhibitor of IRS-1/2 in blocking this pathway in UM. NT157 treatment in UM cells resulted in reduced cell survival and migration, and increased apoptosis. This treatment also significantly inhibited UM tumor growth *in vivo*, in the chicken egg chorioallantoic membrane (CAM) and subcutaneous mouse models, validating the *in vitro* effect. Mechanistically, through reverse phase protein array (RPPA), we identified significant proteomic changes in the PI3K/AKT pathway, a downstream mediator of IGF-1 signaling, with NT157 treatment. Together, these results suggest that NT157 inhibits cell survival, migration *in vitro* and tumor growth *in vivo* via inhibiting IGF-1 signaling in UM.

48 **Introduction**

49 Uveal melanoma (UM) arises from melanocytes in the choroidal plexus of the eye and is
50 biologically different from cutaneous melanoma due to different genetic alterations [1] and a strong
51 tendency to metastasize to the liver [2, 3] (observed in approximately90% of cases with metastasis). The
52 reason for such preferential liver seeding of UM metastatic cells is unknown. Growth factors have been
53 shown to play a significant role in the tissue-specific homing of cancer cells [4]. Liver-borne growth factors,
54 such as the IGF-1 may contribute to this distant metastasis to liver and blocking these factors might have
55 therapeutic value. IGF-1 plays a major role in tumor cell proliferation and survival, and its receptor, IGF-
56 1R, plays a significant role in multi-step process of cancer metastasis [5]. In UM, IGF-1R expression has
57 been shown to be independently prognostic in multi-variate analysis [6]. Also, IGF-1 is one of the major
58 growth factors secreted from the liver, and high IGF-1 serum levels have been shown to be associated with
59 UM metastasis [7].

60 Protein expression of IGF-1R, the receptor for IGF-1, has been detected in UM tumors, and its high
61 expression was shown to be associated with poor survival [8-10]. Despite this high IGF-1R expression, few
62 attempts have been made to target this ligand/receptor system in UM. A phase II trial that targeted IGF-1R
63 in UM with a human monoclonal antibody from IMCLONE (NCI #8832, 2010-0451) [11] did not have any
64 therapeutic benefit and concluded that this monoclonal antibody was not a viable treatment option.
65 Targeting the IGF-1 pathway alone or in combination for more effective therapy regimens against
66 metastatic UM remains to be studied [12]. IRS1/2 are the first downstream targets of activated IGF-1R,
67 which transmit IGF-1R mediated signals. The IRS proteins do not have their own kinase activity, but act
68 as scaffolds for signaling complexes to initiate cellular signaling pathways [13]. IRS-1/2 are intermediates
69 of multiple receptors that control tumor progression and thus can play an important role in the response of
70 tumor cells to different microenvironmental signals. NT157, the small molecule IRS1/2 inhibitor,
71 developed by Dr. Alexander Levitzki, functions by serine phosphorylation and destruction of IRS1 and
72 IRS2, leading to long-term blocking of IGF-1R signaling and strong inhibition of tumor growth [14] in

73 ovarian and prostate cancers as well as BRAF inhibitor resistant melanoma.. The NT compounds are highly
74 effective in anti-cancer activity because they inhibit both the tumor growth promoted by IRS1 and the IRS2-
75 mediated metastasis [15]. Furthermore, inhibition of both IRS proteins precludes the compensation of one
76 for the other [14, 15].

77 In this study, we have utilized both the *in vitro* and *in vivo* models of UM to investigate the effect
78 of IRS-1 inhibition on UM growth, cell survival and migration. Our *in vivo* models, the CAM model and
79 mouse subcutaneous (subQ) xenograft model [16], were previously tested and standardized for studying
80 UM growth inhibition [17]. Here, we show, *in vitro* treatment with NT157 leads to inhibition of UM cell
81 growth, induction of apoptosis and inhibition of cell migration. More significantly, we show inhibition of
82 UM tumor growth on CAM as well as in our subQ mouse model with NT157 treatment.

83

84 **Materials and Methods**

85 **Antibodies and reagents**

86 The IRS-1 antibody for immunohistochemistry analysis was obtained from ABCAM (#ab40777;
87 Abcam, Boston, MA). Similarly, Caspase 3 antibody was obtained from ABCAM (#ab184787). Cell
88 signaling Danvers, MA provided antibodies for Caspase 9 (#9502S); Hexokinase (#2867S), STAT3
89 (#4904S), Phospho STAT 3, (#9131S), Cleaved PARP (#5625S), IRS-1 for western blotting (#2382S),
90 Phospho p38 MAP Kinase (#9215S), p38 MAP Kinase (#9212S), Phospho AKT (#3787S), AKT (#9272S),
91 Phospho Erk1/2(#4376S), Erk1/2 (#9102S) and IGF-1R (#3027S). Phospho IGF-1R antibody was
92 obtained from Sigma Aldrich (SAB4300652; Millipore Sigma, Burlington, MA). The Actin antibody was
93 obtained from Santa Cruz (#sc-47778; Santa Cruz, Dallas, TX). NT157 was obtained from Selleckchem
94 (#NM-4126; Houston, TX).

95 Cell migration assay plates were obtained from Corning (#354578; Corning, Glendale, AZ) and
96 staining Kit was obtained from Siemens (#B4132-1A; Siemens Health care Diagnostic Inc, Newark, DE).
97 MTT reagent was obtained from EMD Millipore Corp (#475989; United Kingdom). Propidium Iodide was

98 procured from Sigma-Aldrich (#81845; Millipore Sigma, Burlington, MA). Ribonuclease A (RNase) was
99 obtained from Sigma-Aldrich (#R4642; Millipore Sigma, Burlington, MA).

100 **Cell culture and treatments**

101 Cell line Mel20–06–039, (RRID:CVCL_8473) [18, 19], was obtained from Dr. Tara A. McCannel.
102 Cell line OMM-1 (RRID:CVCL_6939) [12], Mel202 (RRID: CVCL_C301), 92–1 (RRID: CVCL_8607)
103 [12], and Mel270 (RRID: CVCL_C302) [12] were kindly provided by Drs. Martine Jager and Bruce
104 Ksander. Cell lines obtained from ATCC were: MM28, MP38, MP41, MP46, MP65. Additional UM cell
105 line information is provided in the references [20-23].

106 UM cells were cultured in RPMI 1640 media with 10% FBS, glutamine, Penicillin-streptomycin
107 and Insulin supplement, under ambient oxygen at 37 ^{0}C.

108 **Cell line validation**

109 Cell lines were validated by short random repeat (STR) DNA fingerprinting techniques and
110 mutational analysis, by the MDACC Cancer Center Support Grant (CCSG)-supported Characterized Cell
111 Line Core, using the AmpFLSTR Identifier Kit (Applied Biosystems, Foster City, CA), according to
112 manufacturer's instructions. The STR profiles were compared to known ATCC fingerprints (ATCC.org),
113 and to the Cell Line Integrated Molecular Authentication database (CLIMA) version 0.1.200808
114 (http://bioinformatics.istge.it/clima/). The STR profiles matched known DNA fingerprints or were unique.

115 **Western blotting**

116 Cells were lysed in a buffer containing 50 mM Tris (pH 7.9), 150 mM NaCl, 1% NP40, 1 mM
117 EDTA, 10% glycerol, 1 mM sodium vanadate and a protease inhibitor cocktail (Roche Pharmaceuticals,
118 Nutley, NJ). Proteins were separated by SDS-PAGE with 4-20% gradient gels (Bio-Rad Laboratories,
119 Hercules, CA), transferred to a Hybond-ECL nitrocellulose membrane (GE Healthcare Biosciences,
120 Piscataway, NJ) and blocked in 5% dry milk in PBS. The membrane was then incubated with primary and

121 secondary antibodies, and target proteins were detected with ECL detection reagent (GE Healthcare
122 Biosciences).

123 **FACS Flow cytometry analysis for cell surface expression of IGF-1R**

124 UM cells were washed with phosphate-buffered saline (PBS) and detached by gentle pipetting. The
125 cells were incubated with PE-conjugated mouse monoclonal anti-human IGF-1R antibody (BD
126 Biosciences, Franklin Lakes, NJ) or PE-conjugated isotype-matched control mouse antibody (IgG1k, BD
127 Biosciences) for 1 h on ice and then washed with PBS. The cells were analyzed using FACSCalibur (BD
128 Biosciences), and the data were analyzed using FlowJo software (Tree Star, Inc.).

129 **Propidium Iodide staining and flow cytometry analyses**

130 UM cells were trypsinized, washed and fixed with 70% Ethanol and kept at 4 ^{0}C overnight. Cells
131 were centrifuged and pellet resuspended in PBS to rehydrate for 15 min. Cells were then centrifuged at 500
132 g and treated with 200 µg/mL RNase A for 1 h at 37 ^{0}C. Cells were stained with 40 µg/mL Propidium
133 Iodide for 20 min at room temperature. After centrifugation at 500 x g, cells were resuspended in PBS with
134 0.02% EDTA for cell cycle analysis using a Beckman Coulter Galios 561 analyzer.

135 **Colony formation assay**

136 For the colony formation assay, UM cells were seeded in 24 well plates at 500 cells/well. Next day
137 NT157 (1 and 2.5 µM) was added to the wells. Controls were untreated cells. Cell culture media and NT157
138 were replaced every 3 days. Colonies were allowed to grow until clones in the control wells covered 70-
139 80% of the well surface. For fixing and staining the cells, the culture media was removed, wells washed
140 with 1X PBS to remove dead cells and 1ml of crystal violet in 25% methanol was added. Cells were stained
141 for 5 min at RT. Crystal violet was aspirated and the wells washed with water until crystal violet was
142 removed from everywhere else but the colonies.

143 **Reverse phase protein array (RPPA) analysis**

144 RPPA analyses were performed at the UT MD Anderson Cancer Center's Functional Proteomics
145 RPPA Core facility. Briefly, cell lysates were two-fold serially diluted for five dilutions (from undiluted to
146 1:16 dilution) and arrayed on nitrocellulose-coated slides. Samples were probed with antibodies using
147 catalyzed signal amplification and visualized by 3,3'-diaminobenzidine colorimetric reaction. Slides were
148 scanned on a flatbed scanner to produce 16-bit TIFF images of the reacting spots, and spot densities were
149 quantified using the MicroVigene software program. Relative protein levels for each sample were
150 determined by interpolation of each dilution curves from the "standard curve" constructed by a script in R
151 written by MD Anderson's Department of Bioinformatics & Computational Biology. Heatmaps were
152 generated in Cluster 3.0 (http://www.eisenlab.org/eisen/) as a hierarchical cluster using Pearson correlation
153 and a center metric.

154 **Chicken egg chorioallantoic membrane (CAM) tumor xenograft model**

155 UM cell line 92.1 engineered to express luciferase was engrafted on the CAM for 7 days following
156 previously established methods [24, 25]. Briefly, embryonic day 7 eggs were inoculated with 5 x 10^5 cells
157 in a 1:1 Matrigel and PBS (supplemented with calcium and magnesium) solution. Eggs were randomized
158 into 2 groups with 12 eggs in each set. Three days later, daily vehicle and NT157 (1 μM) treatments were
159 topically applied. Bioluminescence imaging was performed at days 5 and 7 post engraftment using an IVIS
160 Lumina III in vivo imaging system (Perkin Elmer, Waltham, MA). IVIS instrument exposure time was 3
161 seconds, 15 minutes after addition of 15 mg/ml D-luciferin. Region of interest and total flux was determined
162 using the Living Image Software suite. Tumors were imaged and harvested at day 7 post engraftment. Chick
163 embryos were euthanized per AVMA guidelines. CAM tumors were fixed in 10% formalin and embedded
164 in paraffin blocks for downstream immunohistochemical analysis. IHC was performed on paraffin sections
165 of CAM tumors using a pan melanoma antibody cocktail (Biocare Medical, Pacheco, CA).

166 **Cell viability assays**

167 Methylthiazole tetrazolium (MTT)- based cell viability assays were used for estimating cell
168 survival. UM cells were plated at a density of 1×10^4 cells/well in triplicate in a 24-well plate. To assess

169 cell viability, MTT reagent [3-(4,5-dimethylthiazol-2-yl)-2,5-diphenyltetrazolium bromide] (Sigma-
170 Aldrich, St. Louis, MO), dissolved in PBS, was added to a final concentration of 1 mg/mL. After 3 h the
171 precipitate formed was dissolved in DMSO, and the color intensity estimated in a MRX Revelation
172 microplate absorbance reader (Dynex Technologies, Chantilly, VA) at 570 nm.

173 **Cell migration assay**

174 Cell migration assays were performed in Boyden chambers using uncoated filters (BD Biocoat
175 control inserts, BD Biocoat, San Jose, CA). UM cells were plated in 10 cm dishes and treated overnight
176 with NT157 (2.5 μM) or MAB391 (10 μg/ml) for 48 h. Untreated cells were used as control. Next day,
177 1×10^5 cells/well were plated in serum-free medium, and the migration assay done with 10% FBS as chemo-
178 attractant and procedure as described in Chattopadhyay et al., [26]. Stained cells were photographed with a
179 Nikon Eclipse TE2000-U microscope at 20X magnification using NIS Elements advanced research
180 software. To quantify migration, the cells in each filter were counted from five independent fields under
181 the microscope at 40X magnification and the mean cell number/field was calculated. Each assay condition
182 was tested in 2 replicates.

183 **NT157 treatment of subQ UM tumors in NSG mice**

184 For *in vivo* studies UM cell lines, 92.1 and MM28, were grown subcutaneously in NOD *scid* gamma
185 mice. 0.5 x 10^6 UM cells were suspended in 50 μl of HBSS media + growth factor reduced Matrigel (1:1
186 ratio) and subcutaneously injected into the right flank of each mouse. Tumors were measured by slide
187 calipers and allowed to grow to ~75-100 mm^3. The animals were then randomized for treatment with
188 vehicle (40% PEG300 + 5% Tween 80 in water) or NT157 (50 mg/Kg), with 5 animals for each treatment
189 set. Drugs were injected intraperitoneally on alternate days for a total of 3 days each week till end of
190 experiment. Tumor sizes were measured twice every week using slide calipers by blinded observers. All *in*
191 *vivo* studies were performed in accordance with accepted guidelines for housing, euthanasia and treatment,
192 under an Institutional Animal Care and Use Committee-approved protocol at MD Anderson.

193

194 **Results**

195 **IGF-1R and IRS-1 are expressed in uveal melanoma**

196 Since IGF-1 is expressed in highest saturation in the liver [27, 28], and liver is the primary site for
197 UM metastasis [29] we checked the expression of corresponding receptor IGF-1R and the immediate
198 substrate of the receptor activation, IRS-1, in our UM cells and primary tumors. We analyzed 31 unique
199 tumor types and their corresponding normal tissues, including UM tumors from The Cancer Genome Atlas
200 (TCGA) data for IGF-1R gene expression. Each dot on the IGF-1R expression plot (Figure 1A) represents
201 one tumor (red) or normal (green) sample and the samples above the median (expression line) are
202 considered to be overexpressed compared to their corresponding normal tissues. Also, the IGF-1R
203 expression levels are progressively higher moving from left to the right most end of the plot. UM tumors
204 displayed the third highest IGF-1R gene expression amongst cancer types, surpassed only by prostate
205 adenocarcinoma (PRAD) and breast invasive carcinoma (BRCA) (Figure 1A). Next, we screened for IGF-
206 1R RNA and protein expression in validated human UM cell lines representing known genetic backgrounds.
207 All lines showed IGF-1R gene expression as indicated by the RT PCR analysis (Figure 1B), and
208 phosphorylation of IGF-1R was found to be inducible by the ligand, IGF-1, treatment, demonstrating it can
209 be activated in most lines (Figure 1C). Higher expression of IGF-1R was observed in UM cells as compared
210 to non-cancer cell lines (FMC15H melanocytes, HaCaT keratinocytes and BJ fibroblasts) (Figure 1D). The
211 cell surface expression of IGF-1R protein on UM cells was detected by flow cytometry analysis (Figure
212 1E). In order to confirm the expression of downstream pathway components in UM, we investigated the
213 expression of IRS-1, the immediate downstream effector of IGF-1R. Using TCGA data sets, we found IRS-
214 1 transcript expression in UM human patient samples (Figure 2A). Immunohistochemical analysis of IRS-
215 1 protein expression in a matched set of primary and metastatic UM tissues, from the eye and the liver, are
216 shown in Figure 2B. Therefore, UM cells express both IGF-1R and IRS-1 in detectable levels.

217 **IRS-1 inhibiton reduces survival, induces apoptosis, and inhibits migration of UM cells**

218 Small molecule inhibitor NT157 inhibits its target, IRS-1, by protein degradation [14]. We treated
219 UM cells expressing IRS-1 with NT157 to inhbit IRS-1 activity, and observed a reduction in IRS-1 protein
220 levels as shown in western blots (Figure 2C). Since reduction in IRS-1 is expected to affect cell survival
221 [15] so we tested the effect of NT157 on UM cell survival. Through MTT assays we observed inhibition of
222 cell survival in all cell lines tested (Figure 2D). UM cell lines varied in sensitivity to NT157 treatment (2.5
223 μM), ranging between 40%-85% reduction in cell survival. We also corroborated the above observation
224 through the colony formation assay. We treated MEL202, 92.1, MM28, MP38, MP41, MP46, MP65 UM
225 cell lines with NT157 in the colony formation assay, and observed inhibition of colony growth or reduction
226 in colony number (Figures 2E and S2). We again observed varied sensitivities to NT157 among the cell
227 lines tested.

228 We also observed that NT157 induces apoptosis in UM cells, as evident from dose-dependent
229 increase in sub G1 population upon NT157 treatment, observed through FACS analysis after propidium
230 idodide staining (Figure 2F and Table 1). To charecterize whether this G0/G1 cell accumulation is due to
231 apoptosis, we performed molecular analysis of apoptotic marker using western blotting. We observed
232 increased levels of PARP processing (cleaved PARP induction) as well as caspase 3 processing (reduction
233 in caspase 3 protein levels) after NT157 treatment of UM cell lines (western blots, Figure 2G).

234 As IGF-1 pathway is a known modulator of cell migration [30], we tested the effect of IRS-1
235 inhibiton on UM cell migration. The UM cell lines treated with NT157 overnight were subjected to a
236 Boyden Chamber-type cell migration assay with 10% FBS as the chemo-attractant. Significantinhibition
237 of cell migration was observed in NT157-treated UM cells (Figures 2H and S1B).

238 We also compared the efficacy of NT157 in its ability to block different cellular/physiological
239 processes against a neutralizing, monoclonal antibody to IGF-1R (MAB391). After confirming MAB391
240 targets IGF-1R activation (Figure S1A), we compared the effect of MAB391 vs. NT157 in cell viablity and
241 migration assays. NT157 was more effective in blocking UM cell survival in an MTT-based assay in the
242 two cell lines tested (Figure S1B) when compared with MAB391. Similarly, in an *in vitro* migration assay,

243 NT157 performed better in cell migration inhibition in response to 10% fetal bovine serum (Figure S1C).
244 Overall, NT157 blocks the physiological functions of IGF-1/IGF-1R pathway in UM cells with high
245 efficiency.

246 **Multiple cellular pathways are modulated in response to IRS-1 inhibition**

247 Since IGF-1R affects several different signaling pathways in the cells, we wanted to understand
248 how the major cellular signaling pathways in UM cells will be affected by NT157 treatment. Proteomic
249 analysis with Reverse Phase Protein Array (RPPA) was performed after treatment of four different UM cell
250 lines with two NT157 doses (1 μM and 2.5 μM) and for two different time intervals (24 and 48 h). RPPA
251 data analysis of NT157-treated vs. untreated UM cells demonstrated several changes in major cell signaling
252 pathways. We observed dose- and time-dependent increases in p85, the inhibitory subunit of PI3K catalytic
253 activity compared to untreated samples, which indicates reduced activation of PI3K pathway. We also
254 observed minimal increase in the activation of MAPK pathways, and changes in cell cycle effectors and
255 increase in hexokinase-II levels as shown in Figure 3A. To validate the signaling pathway changes from
256 RPPA results, we used wesern blotting on an independent set of samples to detect significant changes
257 observed. Hexokinase-II seemed to increase in an NT157 dose-dependent manner in all cell lines tested.
258 Similarly, JNK unformly decreased with increase in NT157 dose. At higher concentration (2.5 μM) and
259 longer timepoint (48 h) AKT activation was effectively reduced (Figure 3B). Therefore, this data shows a
260 reduction in overall activated levels of PI3K/AKT pathway upon NT157 treatment, indicating an inhibitory
261 effect of NT157 on UM cell survival.

262 **IRS-1 targeting reduces UM tumor growth in a chicken CAM model**

263 The chicken CAM has been previously used as a successful *in vivo* system to model UM xenograft
264 growth [17, 31]. To test the effect of IRS-1 inhibition on tumor progression *in vivo*, we engrafted luciferase-
265 tagged 92.1 cells (a UM cell line) on the chicken CAM to generate UM xenografts. After confirming that
266 the tumors generated on the CAM model are of melanoma origin by pan-melanoma marker staining
267 (HMB1, Tyrosinase and S100) (Figure 4A), we treated the resulting tumors with different concentrations

268 of NT157. Gross tumor analysis demonstrates a reduction in overall tumor growth in response to NT157
269 treatment (Figure 4B).The bioluminescence-based quantification of tumor progression showed that NT157
270 decreased total flux compared to the vehicle controls (Figures 4C and D). This suggests a tumor size
271 decrease with NT157 treatment. These results suggest that inhibiting IRS1/2 can block UM tumor growth.

272 **Inhibition of IRS-1 significantly reduces UM tumor growth in mice**

273 To complement the chicken CAM model data, the efficacy of targeting IRS-1 using NT157 was
274 also examined using subcutaneous UM models in mice (see Materials and Methods). Xenograft tumors
275 were generated using the UM cell lines 92.1 and MM28 in NSG mice. Five mice were treated with vehicle
276 and five others with NT157. Treatment with NT157 strongly suppressed UM tumor growth as compared
277 to the untreated control models (Figures 5A and C). Significant differences between the NT157 and vehicle-
278 treated groups were also observed in the average UM xenograft tumor weight at the end of the experiments
279 (Figure 5B). Therefore, in these experiments, we validated *in vivo* the inhibitory effect of IRS-1 blocking
280 on tumor cell growth. There were no significant changes in the average body weights of mice in the NT157-
281 treated vs. vehicle-treated group demonstrating that the dose of NT157 chosen for treatment was well
282 tolerated.

283

284 **Discussion**

285 Previously, we targeted IGF-1R in UM in a phase II trial with IMC-A12, a human monoclonal
286 antibody to the receptor [11], and we did not observe any responders and concluded that this monoclonal
287 antibody was not a viable treatment option. However, our *in vitro* experiments with this antibody showed
288 inhibition of IGF-1R activation and cell migration [11]. In the clinical setting, monoclonal antibodies may
289 not affect functional aspects of cell survival efficiently [32], because antibody uptake by the tumor depends
290 on the balance between pharmacokinetics and efficient penetration as well as retention in the targeted tissue.

291 Therefore, here, we evaluated NT157, a small molecule inhibitor of IRS-1/2, the substrates immediately
292 downstream to IGF-1R, in this study.

293 After confirming IGF-1R expression in UM tumors from our preliminary TCGA analysis (Figure
294 1A), we also observed IGF-1R over-expression in all UM cell lines tested (Figure 1B). Higher expression
295 of IGF-1R in the UM cells compared to non-cancerous cells (Figure 1D) shows that targetting IGF-1R in
296 patients may circumvent toxicity challenges. IRS-1 inhibition, using NT157, successfully blocked UM cell
297 survival, cell migration and induced apoptosis in UM cells (Figure 2). Our RPPA analysis, post -NT157
298 treatment, identified key signaling pathways/proteins that were altered upon IRS-1 inhibition in UM (Figure
299 3). Most importantly, we observed an increase in protein levels of p85 subunit of PI3K, indicating lower
300 PI3K activation upon NT157 treatment. Since PI3K/AKT pathway promotes cell survival, reduced
301 activation of this pathway might contribute to tumor growth inhibition, as evident from our *in vivo* data
302 (Figures 4 and 5). We also observed changes in protein levels of other cell signaling pathways (hexokinase-
303 II, MAPK, ribosomal protein S6 [RPS6], and STAT3) upon NT157 treatment (Figure 3A), however these
304 genes were not associated with overall UM survival (data not shown) when we analyzed the TCGA data
305 sets [33]. For these markers, we compared low (below median expression) and high (above median) groups
306 and found no statistically significant associations.

307 We also compared a monoclonal neutralizing antibody of IGF-1R against NT157 in their capacity
308 to block UM cell survival and UM cell migration (Figure S1). Cancer cell migration is an important step
309 for disease progression and metastasis. Since, UM with primary tumor in the eye shows distant metastasis
310 to liver (>90%) [2, 3], liver-borne IGF-1 may play a major role in UM cell migration. We have shown that
311 NT157 performs better than the monoclonal antibody in each of these assays and is therefore, a better
312 candidate for inhibiting IGF-1/IGF-1R signaling in UM cell models (Figure S1). The success of a
313 therapeutic strategy involving a small molecule, or an antibody depends on multiple factors like uptake,
314 bioavailability, and stability of the agent under physiological conditions. Therefore, it is important to test
315 both these avenues, pre-clinically, to develop the most effective or suitable therapeutic strategy.

316 Most importantly, we validated the *in vitro* inhibitory effect of NT157 on UM cell survival using
317 *in vivo* models for UM tumor growth. Tumor growth reduction in a chicken CAM model of UM with NT157
318 treatment clearly shows that blocking the IGF-1/IGF-1R axis in UM is beneficial in controlling tumor
319 growth (Figure 4). Similarly, in our subQ mouse model of UM tumor growth, NT157 treatment resulted in
320 reduction of tumor volume and tumor weight (Figure 5). Since NT157 is not a clinical compound, our study
321 forms the basis or proof-of-concept for targeting IGF-1/IGF-1R in a clinical setting in UM.

322 In conclusion, our results suggest blocking IGF-1/IGF-1R axis in UM inhibits cell survival, cell
323 migration, and induces apoptosis *in vitro*. Targeting this pathway *in vivo* inhibits UM tumor growth. Recent
324 FDA approval of Tebentafusp for use in non-resectable UM [34, 35] has generated hope and created a
325 therapeutic option for a section of the metastatic UM patients. Since this is the only approved therapy and
326 one size does not fit all (tebentafusp only is applicable to HLA-A*02:01-positive adult patients) , there is
327 an urgent need to develop new therapeutic strategies. Our results strongly support the rationale to develop
328 clinical studies based on IGF-1/IGF-1R inhibition in UM. Considering the fact that single-agent therapies
329 often do not produce durable responses in melanoma, the future therapeutic strategies blocking IGF-1/IGF-
330 1R axis may need to consider combination therapies for a synergistic effect to control tumor growth.

331

332 **Author contributions:** Concept and design: CC, EAG; Acquisition of data: CC, Rajat Bhattacharya, YQ,
333 FSK, GAW, HV, and Rishav Bhattacharya; Chicken CAM model-based study design and execution: GAW
334 and HV; High throughput drug screening and analyses: CS and PR, respectively; Analysis and interpretation
335 of data: CC, JR, SP, and HV; Writing, review, and/or revision of the manuscript: CC, JR, SP, HV, and
336 EAG; Study supervision: CC

337

338 **Competing Interests:** None to report.

339

Funding: This research was supported by the Dr. Miriam and Sheldon G. Adelson Medical Research Foundation, MD Anderson Melanoma SPORE (P50CA221703), and funding from The Mulva family Foundation.

Acknowledgements: We thank Dr. Sirisha Yadugiri for manuscript reviewing and editing, and Mrs. Violet Garcia for manuscript formatting and administrative support. We thank Dr. Michael A. Davies for scientific advice and critical review to improve the quality of the manuscript. We also thank The UT MD Anderson Flow Cytometry and cellular imaging facility, which is supported in part by NIH through the MD Anderson Cancer Center support grant CA016672, for providing support for FACS analysis and imaging. We thank The Patient-Derived Xenograft and Advanced in vivo Models Core Facility, which is supported in part by NIH through the Baylor College of Medicine Cancer Center support grant #2P30CA125123-14. We also thank The UT MD Anderson RPPA core, supported by NCI grant # CA16672 and NIH grant R50CA221675, for RPPA data analysis.

Data Availability Statement: All relevant data are available from the corresponding author upon request.

References:

1 Horsman DE, White VA. Cytogenetic analysis of uveal melanoma. Consistent occurrence of monosomy 3 and trisomy 8q. *Cancer* 1993; 71: 811-819.

2 Lorigan JG, Wallace S, Mavligit GM. The prevalence and location of metastases from ocular melanoma: imaging study in 110 patients. *AJR Am J Roentgenol* 1991; 157: 1279-1281.

3 Yang H, Fang G, Huang X, Yu J, Hsieh CL, Grossniklaus HE. In-vivo xenograft murine human uveal melanoma model develops hepatic micrometastases. *Melanoma Res* 2008; 18: 95-103.

363 4 Witsch E, Sela M, Yarden Y. Roles for growth factors in cancer progression. *Physiology (Bethesda)*
364 2010; 25: 85-101.

365 5 Bähr C, Groner B. The IGF-1 receptor and its contributions to metastatic tumor growth-novel
366 approaches to the inhibition of IGF-1R function. *Growth Factors* 2005; 23: 1-14.

367 6 Economou MA, All-Ericsson C, Bykov V, Girnita L, Bartolazzi A, Larsson O *et al*. Receptors for
368 the Liver Synthesized Growth Factors IGF-1 and HGF/SF in Uveal Melanoma: Intercorrelation
369 and Prognostic Implications. *Investigative Ophthalmology & Visual Science* 2005; 46: 4372-4375.

370 7 Frenkel S, Zloto O, Pe'er J, Barak V. Insulin-like growth factor-1 as a predictive biomarker for
371 metastatic uveal melanoma in humans. *Invest Ophthalmol Vis Sci* 2013; 54: 490-493.

372 8 Economou MA, All-Ericsson C, Bykov V, Girnita L, Bartolazzi A, Larsson O *et al*. Receptors for
373 the liver synthesized growth factors IGF-1 and HGF/SF in uveal melanoma: intercorrelation and
374 prognostic implications. *Acta Ophthalmol* 2008; 86 Thesis 4: 20-25.

375 9 Topcu-Yilmaz P, Kiratli H, Saglam A, Söylemezoglu F, Hascelik G. Correlation of
376 clinicopathological parameters with HGF, c-Met, EGFR, and IGF-1R expression in uveal
377 melanoma. *Melanoma Res* 2010; 20: 126-132.

378 10 All-Ericsson C, Girnita L, Seregard S, Bartolazzi A, Jager MJ, Larsson O. Insulin-like growth
379 factor-1 receptor in uveal melanoma: a predictor for metastatic disease and a potential therapeutic
380 target. *Invest Ophthalmol Vis Sci* 2002; 43: 1-8.

381 11 Mattei J, Ballhausen A, Bassett R, Shephard M, Chattopadhyay C, Hudgens C *et al*. A phase II
382 study of the insulin-like growth factor type I receptor inhibitor IMC-A12 in patients with metastatic
383 uveal melanoma. *Melanoma Res* 2020; 30: 574-579.

384 12 Luke JJ, Triozzi PL, McKenna KC, Van Meir EG, Gershenwald JE, Bastian BC *et al*. Biology of
385 advanced uveal melanoma and next steps for clinical therapeutics. *Pigment Cell Melanoma Res*
386 2015; 28: 135-147.

387 13 Mardilovich K, Pankratz SL, Shaw LM. Expression and function of the insulin receptor substrate
388 proteins in cancer. *Cell Communication and Signaling* 2009; 7: 14.

389 14 Reuveni H, Flashner-Abramson E, Steiner L, Makedonski K, Song R, Shir A *et al*. Therapeutic
390 destruction of insulin receptor substrates for cancer treatment. *Cancer Res* 2013; 73: 4383-4394.

391 15 Shaw LM. The insulin receptor substrate (IRS) proteins: at the intersection of metabolism and
392 cancer. *Cell Cycle* 2011; 10: 1750-1756.

393 16 Richards JR, Yoo JH, Shin D, Odelberg SJ. Mouse models of uveal melanoma: Strengths,
394 weaknesses, and future directions. *Pigment Cell Melanoma Res* 2020; 33: 264-278.

395 17 Kalirai H, Shahidipour H, Coupland SE, Luyten G. Use of the Chick Embryo Model in Uveal
396 Melanoma. *Ocul Oncol Pathol* 2015; 1: 133-140.

397 18 Burgess BL, Rao NP, Eskin A, Nelson SF, McCannel TA. Characterization of three cell lines
398 derived from fine needle biopsy of choroidal melanoma with metastatic outcome. *Mol Vis* 2011;
399 17: 607-615.

400 19 von Euw E, Atefi M, Attar N, Chu C, Zachariah S, Burgess BL *et al*. Antitumor effects of the
401 investigational selective MEK inhibitor TAK733 against cutaneous and uveal melanoma cell lines.
402 *Mol Cancer* 2012; 11: 22.

403 20 De Waard-Siebinga I, Blom DJ, Griffioen M, Schrier PI, Hoogendoorn E, Beverstock G *et al*.
404 Establishment and characterization of an uveal-melanoma cell line. *Int J Cancer* 1995; 62: 155-
405 161.

406 21 Jager MJ, Magner JA, Ksander BR, Dubovy SR. Uveal Melanoma Cell Lines: Where do they come
407 from? (An American Ophthalmological Society Thesis). *Trans Am Ophthalmol Soc* 2016; 114: T5.

408 22 Ksander BR, Rubsamen PE, Olsen KR, Cousins SW, Streilein JW. Studies of tumor-infiltrating
409 lymphocytes from a human choroidal melanoma. *Invest Ophthalmol Vis Sci* 1991; 32: 3198-3208.

410 23 Verbik DJ, Murray TG, Tran JM, Ksander BR. Melanomas that develop within the eye inhibit
411 lymphocyte proliferation. *Int J Cancer* 1997; 73: 470-478.

412 24 DeBord LC, Pathak RR, Villaneuva M, Liu HC, Harrington DA, Yu W *et al*. The chick
413 chorioallantoic membrane (CAM) as a versatile patient-derived xenograft (PDX) platform for
414 precision medicine and preclinical research. *Am J Cancer Res* 2018; 8: 1642-1660.

415 25 Villanueva H, Sikora AG. The Chicken Embryo Chorioallantoic Membrane (CAM): A Versatile
416 Tool for the Study of Patient-Derived Xenografts. *Methods Mol Biol* 2022; 2471: 209-220.

417 26 Chattopadhyay C, El-Naggar AK, Williams MD, Clayman GL. Small molecule c-MET inhibitor
418 PHA665752: effect on cell growth and motility in papillary thyroid carcinoma. *Head Neck* 2008;
419 30: 991-1000.

420 27 Abdel-Wahab R, Shehata S, Hassan MM, Habra MA, Eskandari G, Tinkey PT *et al*. Type I insulin-
421 like growth factor as a liver reserve assessment tool in hepatocellular carcinoma. *J Hepatocell*
422 *Carcinoma* 2015; 2: 131-142.

423 28 Maki RG. Small is beautiful: insulin-like growth factors and their role in growth, development, and
424 cancer. *J Clin Oncol* 2010; 28: 4985-4995.

425 29 Awh CC, Wilson MW. Symptomatic Liver Metastasis Prompting Diagnosis of Uveal Melanoma.
426 *Ocul Oncol Pathol* 2020; 6: 164-167.

427 30 Grimberg A. Mechanisms by which IGF-I may promote cancer. *Cancer Biol Ther* 2003; 2: 630-
428 635.

429 31 Sokolenko EA, Berchner-Pfannschmidt U, Ting SC, Schmid KW, Bechrakis NE, Seitz B *et al*. Optimisation of the Chicken Chorioallantoic Membrane Assay in Uveal Melanoma Research. *Pharmaceutics* 2021; 14.

432 32 Chames P, Van Regenmortel M, Weiss E, Baty D. Therapeutic antibodies: successes, limitations and hopes for the future. *Br J Pharmacol* 2009; 157: 220-233.

434 33 Robertson AG, Shih J, Yau C, Gibb EA, Oba J, Mungall KL *et al*. Integrative Analysis Identifies Four Molecular and Clinical Subsets in Uveal Melanoma. *Cancer Cell* 2017; 32: 204-220.e215.

436 34 Liu AW, Wei AZ, Maniar AB, Carvajal RD. Tebentafusp in advanced uveal melanoma: proof of principle for the efficacy of T-cell receptor therapeutics and bispecifics in solid tumors. *Expert Opin Biol Ther* 2022; 22: 997-1004.

439 35 Nathan P, Hassel JC, Rutkowski P, Baurain JF, Butler MO, Schlaak M *et al*. Overall Survival Benefit with Tebentafusp in Metastatic Uveal Melanoma. *N Engl J Med* 2021; 385: 1196-1206.

441

442 **Figure Legends:**

443 **Figure 1. Expression of IGF-1R in UM tumors and cell lines.** (**A**) The IGF-1R mRNA expression levels
444 in tumor and normal tissues were compared in 33 cancer (red dots) and corresponding normal (green dots)
445 tissues through TCGA database analysis. The expression in UM is indicated by an arrow. (**B**) RT-PCR
446 analyses showing IGF-1R mRNA levels in 10 different UM cell lines. (**C**) Western blot analysis showing
447 IGF-1R activation/induction in UM cell lines with 75 ng/mL of IGF-1 treatment. (**D**) Western blot analysis
448 for IGF-1R levels using IGF-1R antibody shows higher expression of IGF-1R protein in UM cell lines (92.1
449 and Mel270) *versus* non-cancerous melanocytes, keratinocytes and fibroblasts. (**E**) FACS histogram plots
450 showing cell surface expression of IGF-1R in the UM cell lines (Mel285), Mel202, 92.1, OMM2.3, OMM1,
451 39, 70 and 196) stained with IGF-1R antibody (red lines). The isotype control is represented by the black
452 lines in the FACS histograms.

453 **Figure 2. NT157 treatment reduces IRS-1 levels leading to reduction of cell viability, migration and**
454 **induction of apoptosis in UM cell lines.** (**A**) TCGA dataset analysis shows high expression of IRS-1
455 mRNA in UM tumors (indicated by an arrow) among 33 cancer (red dots) and corresponding normal (green
456 dots) tissues. (**B**) Immunohistochemical staining of matched primary (eye) and metastatic (liver) UM tumor
457 tissues using IRS-1 antibody detects IRS-1 expression in both eye and liver. (**C**) Western blot analysis of
458 cell extracts from UM cell lines (92.1, OMM2.5, OMM1, MEL20-06-039, MP65) treated with NT157 (1
459 μM) and probed with anti-IRS-1 antibody shows IRS-1 protein levels decrease in UM cell lines with NT157
460 treatment. (**D**) Quantification of percent cell survival using MTT-based assays in UM cell lines (MP46,
461 MM28, MEL202, 92.1, MP65 and MP41) with (0.05, 0.1, 0.25, 0.5, 1.0, 2.5 μM) or without NT157
462 treatment shows NT157 dose-dependent decrease in cell survival. The bar graphs represent percentage of
463 cell survival and are a mean ± SD of three independent experiments. (**E**) **Colony formation assay:**
464 Representative images of crystal violet staining shows fewer number of colonies formed by UM cell lines
465 (MP46, MM28, MEL202, 92.1, MP65 and MP41) with NT157 treatment (1 and 2.5 μM) compared to
466 untreated controls. (**F**) Representative FACS histograms of DNA content detected by propidium iodide
467 staining to detect cell cycle status in UM cell lines (MP46, MM28 and MEL20-06-039 and MP65) shows
468 a dose-dependent increase of number of cells in G0/G1 phase with NT157 treatment (1 and 2.5 μM) *vs.* no
469 treatment. (**G**) Western blot analysis of total cell extracts shows NT157 dose-dependent (1 and 2.5 μM)
470 increase in cleaved PARP and decrease in caspase3 levels detected by respective antibodies in UM cell
471 lines (MEL202, MEL270, 92.1 and MEL20-06-039) compared to untreated controls. (**H**) Quantification of
472 cell migration in UM cell lines (OMM1, 92.1, MEL202, MP65 and MM28) shows reduction in migration
473 of cells treated with NT157 (2.5 μM) compared to untreated controls. An average of five fields of cells/filter
474 were counted under a microscope with 40X magnification. The average number of cells counted/field were
475 obtained in two independent experiments and the mean ± SD of these average cell counts/ field were plotted
476 as bar graphs.

477 **Figure 3**. **Significant changes in cell signaling proteins detected post-NT157 treatment.** (**A**) RPPA
478 protein profiling of four 4 UM cell lines (MEL270, MM28, MEL-20-06-039 and 92.1; represented by each
479 dot). The RPPA expression values are displayed on the y-axis for antibodies that show a significant
480 difference ($P < 0.05$) compared to control sample. Cells were treated either for 24 or 48 hours with a 1 or
481 2.5 μM concentration of NT157. Green dots represent untreated cells; orange and red dots represent cells
482 treated with 1 and 2.5 μM of NT157, respectively for 24 and 48 h. (**B**) Western blot analyses to validate
483 some of the significant changes observed in RPPA using antibodies against hexokinase-II, phospho-AKT,
484 and JNK2 shows treatment and time-dependent (1 and 2.5 μM for 24 and 48 h) upregulation of hexokinase-
485 II and downregulation of phospho-AKT.

486 **Figure 4. NT157 treatment reduces UM tumor growth in the chicken CAM model.** (**A**) H&E (left) and
487 pan-melanoma cocktail (anti- HMB1, Tyrosinase and S100 antibodies; right) staining of UM tumor tissues
488 from 92.1 cells grown in chicken CAM model show the presence of melanoma cells. Representative (20x)
489 and high magnification (inlay 2x) images shown as described. (**B**) Brightfield images of vehicle-treated
490 (upper panel) and NT157-treated (1 μM; lower panel) representative tumors (two representative images per
491 treatment) show a reduction of tumor size with NT157 treatment. (**C**) Representative bioluminescence
492 images of chicken eggs bearing luciferase-tagged UM cells (92.1) treated with vehicle controls (left panel)
493 or NT157 (1 μM) (right panel). (**D**) Tumor size of the implants was calculated as the total flux (photons per
494 second) from the images in (C), which shows a reduction in tumor size with NT157 treatment; mean ± SD
495 of three independent experiments was plotted as a graph; $*P = 0.022$.

496 **Figure 5. NT157 treatment inhibits UM tumor growth in a SubQ mouse model**. Subcutaneous tumors
497 grown in NSG mice with 0.5 million UM cells 92.1 (top) and MM28 (bottom) were treated intraperitoneally
498 with NT157 (50 mg/kg body weight), 3 times per week after tumors reached ~100 mm size. Tumor volume
499 was measured twice weekly with slide calipers. When more than 2 tumors reached 1000 mm^3 volume in
500 any one group, the experiment was ended and tumors were harvested. (**A**) Shows harvested tumors from
501 untreated and NT157 treated groups at the endpoint. (**B**) Shows a reduction in collective tumor weight at

502 the endpoint and (**C**) time-depedent reduction in tumor volume with NT157 treatement (1 μM) vs. untreated
503 controls. The data points marked ** and *show $P < 0.01$ and <0.05, respectively.

504

505 **Tables:**

506 **Table 1. Shows percent cells gated in subG1 phase with /without treatment with NT157**. The percent
507 of cells in cell cycle phases were obtained by counting propidium iodide stained cells after 48 h of NT157
508 treatment. At the higher NT157 concentration we see an accumulation of subG1 cells compared to the
509 untreated controls.

510

511 **Supplemental Figures:**

512 **Supplemental Figure 1. NT157 is more efficient in inhibiting UM cell survival and migration**
513 **compared to anti-IGF-1R antibody.** (**A**) Western blot analysis of IGF-1R activation with MAB391 in
514 UM cells (MEL20-06-039 and MEL270 cell lines) shows dose and time-dependent inhibition of IGF-1R
515 phosphorylation, confirming the specificity of the antibody. (**B**) Quantification of cell survival measured
516 through MTT-based assay after treatment of UM cells (MEL20-06-039 and MEL270 cell lines) with
517 MAB391(left) or NT157 (right) or vehicle control, shows NT157 is more effective in blocking UM cell
518 survival compared to MAB391. The bar graphs represent percent survival and mean ± SD of three
519 independent experiments were plotted. (**C**) An *in vitro* cell migration assay shows the staining of migrated
520 UM cells (MEL20-06-039, MEL270, MEL285 cell lines; left). The quantification of stained cells (right)
521 shows NT157 (2.5 μM) treatment blocks cell migration more efficiently than MAB391 (100 ng/mL) or
522 vehicle controls. Bar graphs represent the mean ± SD of average number of cells counted/field from 5 fields
523 per condition, in two independent set of experiments.

524 **Supplemental Figure 2. Effect of NT157 on UM cell survival in a colony formation assay.** The average
525 number of colonies counted after staining with crystal violet in NT157 treated (1 and 2.5 μM) and untreated

526 control UM cell lines (MM28, MEL202, MP38, MP41, 92.1, MP46, MP65) were plotted, which shows
527 dose-dependent inhibition of UM cell survival with NT157 treatment. A total of 5 fields/condition/cell line
528 were counted to obtain the average number of colonies, in two independent set of experiments.

Figure 1

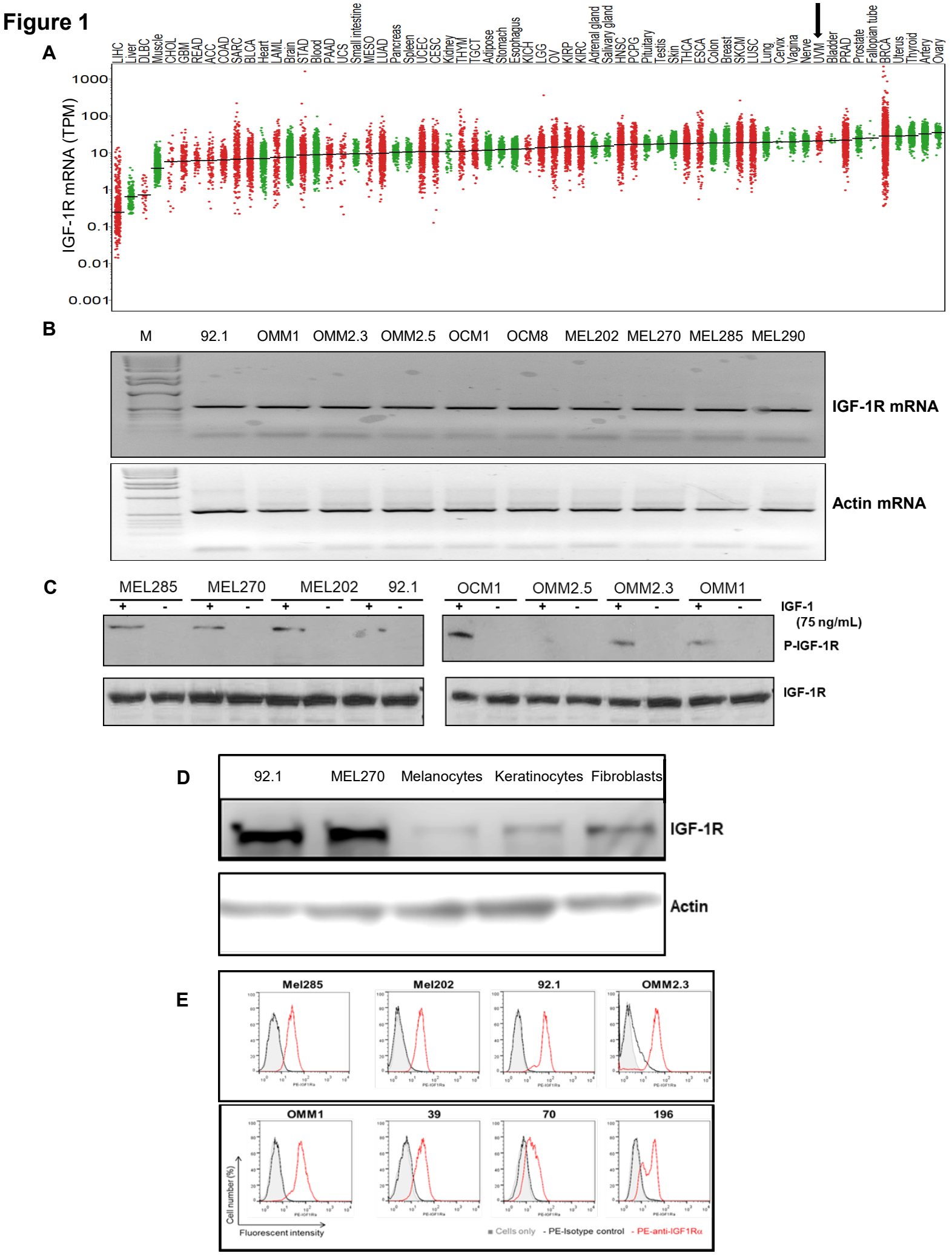
A
IGF-1R mRNA (TPM)
1000
100
10
1
0.1
0.01
0.001
LHC Liver DLBC Muscle CHOL GBM READ ACC COAD SARC BLCA Heart LAML Brain STAD Blood PAAD UCS Small intestine MESO LUAD Pancreas Spleen UCEC CESC Kidney THYM TGCT Adipose Stomach Esophagus KICH LGG OV KIRP KIRC Adrenal gland Salivary gland HNSC PCPG Pituitary Testis Skin THCA ESCA Colon Breast SKCM LUSC Lung Cervix Vagina Nerve UVM Bladder PRAD Prostate Fallopian tube BRCA Uterus Thyroid Artery Ovary
B
M 92.1 OMM1 OMM2.3 OMM2.5 OCM1 OCM8 MEL202 MEL270 MEL285 MEL290
IGF-1R mRNA
Actin mRNA
C
MEL285 MEL270 MEL202 92.1 OCM1 OMM2.5 OMM2.3 OMM1
+ - + - + - + - + - + - + - + -
IGF-1 (75 ng/mL)
P-IGF-1R
IGF-1R
D
92.1 MEL270 Melanocytes Keratinocytes Fibroblasts
IGF-1R
Actin
E
Mel285 Mel202 92.1 OMM2.3
OMM1 39 70 196
Cell number (%)
Fluorescent intensity
Cells only - PE-Isotype control - PE-anti-IGF1Rα

Figure 2

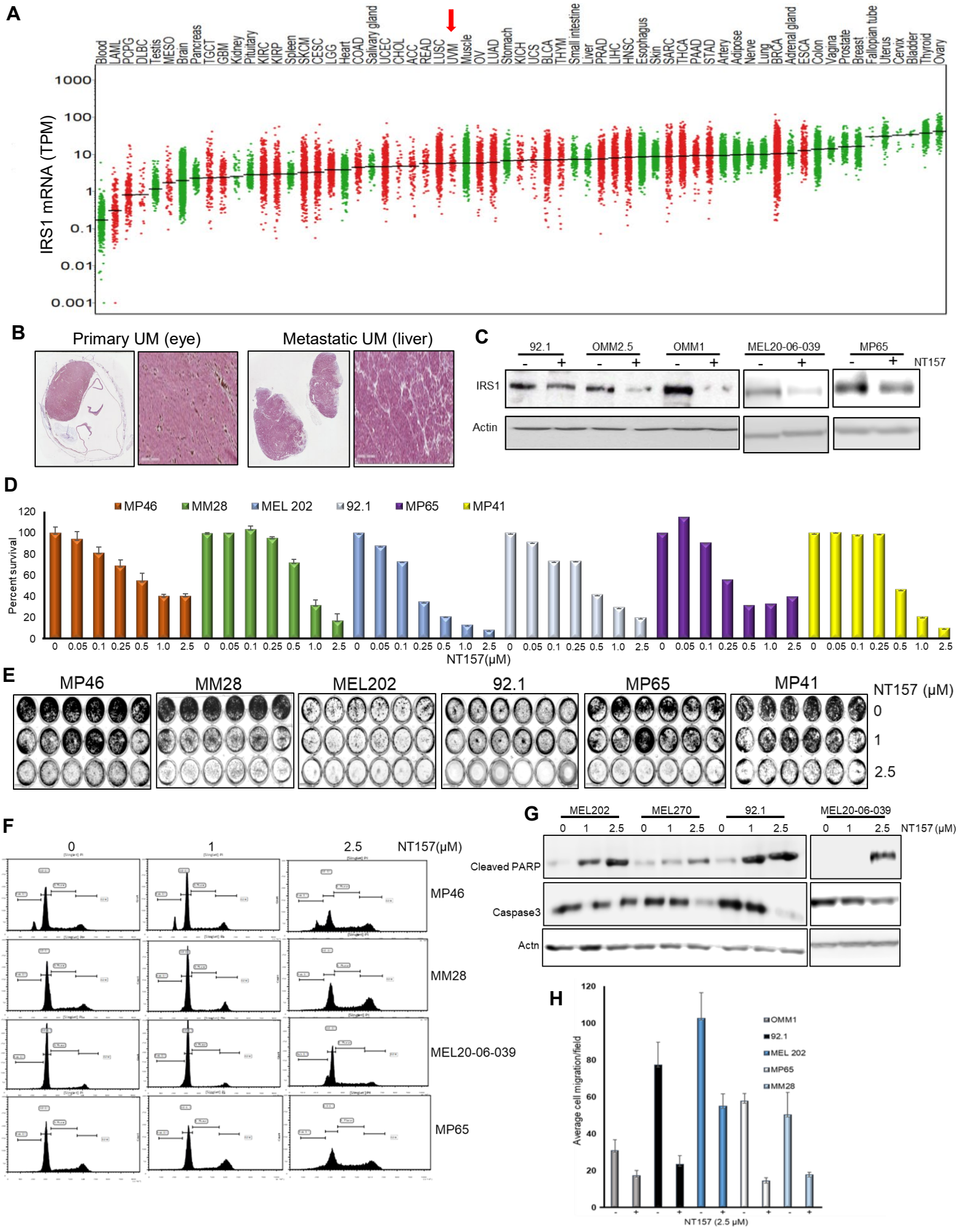
A
IRS1 mRNA (TPM)
1000
100
10
1
0.1
0.01
0.001
Blood LAML PCPG DLBC Testis MESO Brain Pancreas TGCT GBM Kidney Pituitary KIRC KIRP Spleen SKCM CESC LGG Heart COAD Salivary gland UCEC CHOL ACC READ LUSC UVM Muscle OV LUAD Stomach KICH UCS BLCA THYM Small intestine Liver PRAD LIHC HNSC Esophagus Skin SARC THCA PAAD STAD Artery Adipose Nerve Lung BRCA Adrenal gland ESCA Colon Vagina Prostate Breast Fallopian tube Uterus Cervix Bladder Thyroid Ovary
B
Primary UM (eye)
Metastatic UM (liver)
C
92.1
OMM2.5
OMM1
MEL20-06-039
MP65
NT157
IRS1
Actin
D
MP46
MM28
MEL 202
92.1
MP65
MP41
Percent survival
NT157(μM)
E
MP46
MM28
MEL202
92.1
MP65
MP41
NT157 (μM)
0
1
2.5
F
0
1
2.5
NT157(μM)
MP46
MM28
MEL20-06-039
MP65
G
MEL202
MEL270
92.1
MEL20-06-039
NT157 (μM)
Cleaved PARP
Caspase3
Actn
H
OMM1
92.1
MEL 202
MP65
MM28
Average cell migration/field
NT157 (2.5 μM)

Figure 3

A

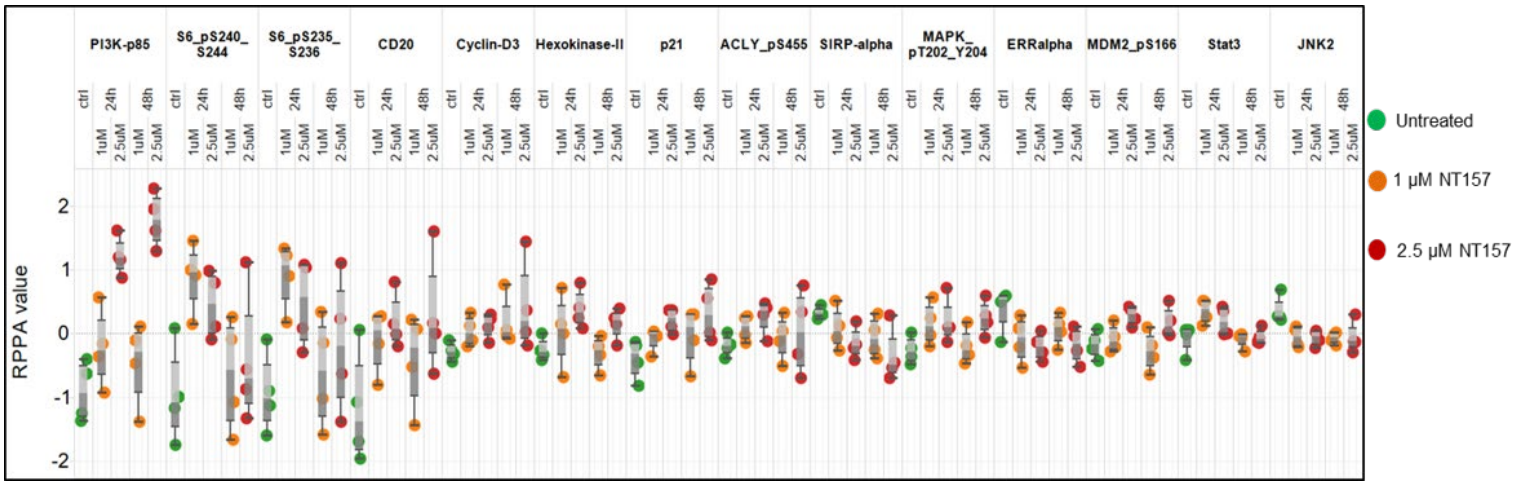
PI3K-p85
S6_pS240_S244
S6_pS235_S236
CD20
Cyclin-D3
Hexokinase-II
p21
ACLY_pS455
SIRP-alpha
MAPK_pT202_Y204
ERRalpha
MDM2_pS166
Stat3
JNK2
ctrl
24h
48h
1uM
2.5uM
RPPA value
2
1
0
-1
-2
Untreated
1 μM NT157
2.5 μM NT157

B

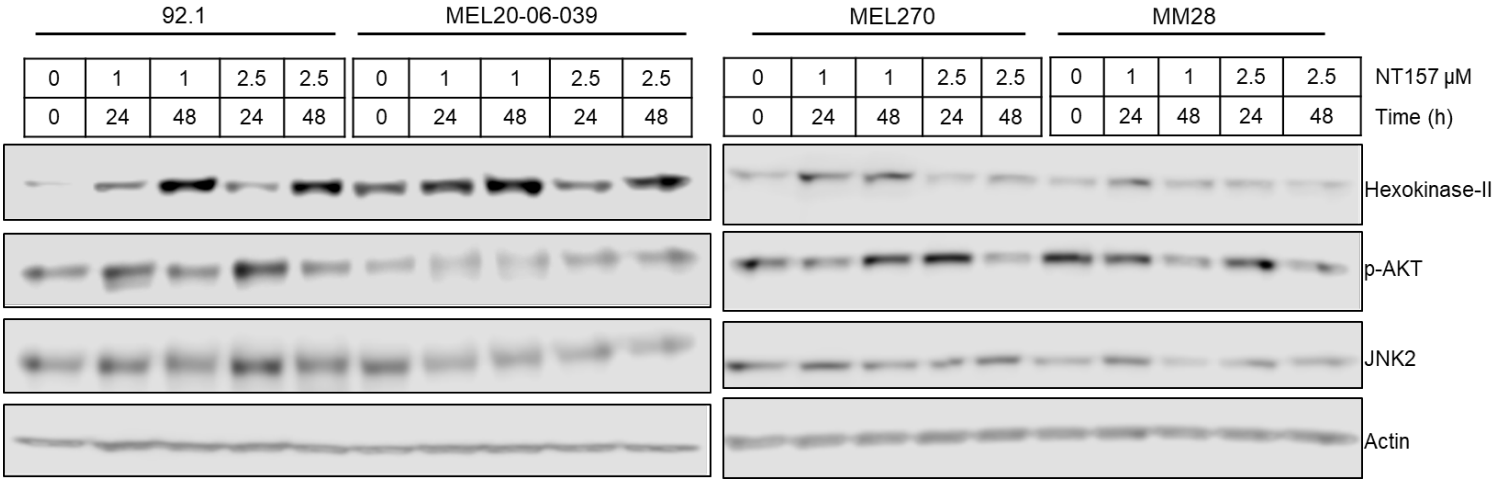
92.1
MEL20-06-039
MEL270
MM28
NT157 μM
Time (h)
Hexokinase-II
p-AKT
JNK2
Actin

Figure 4

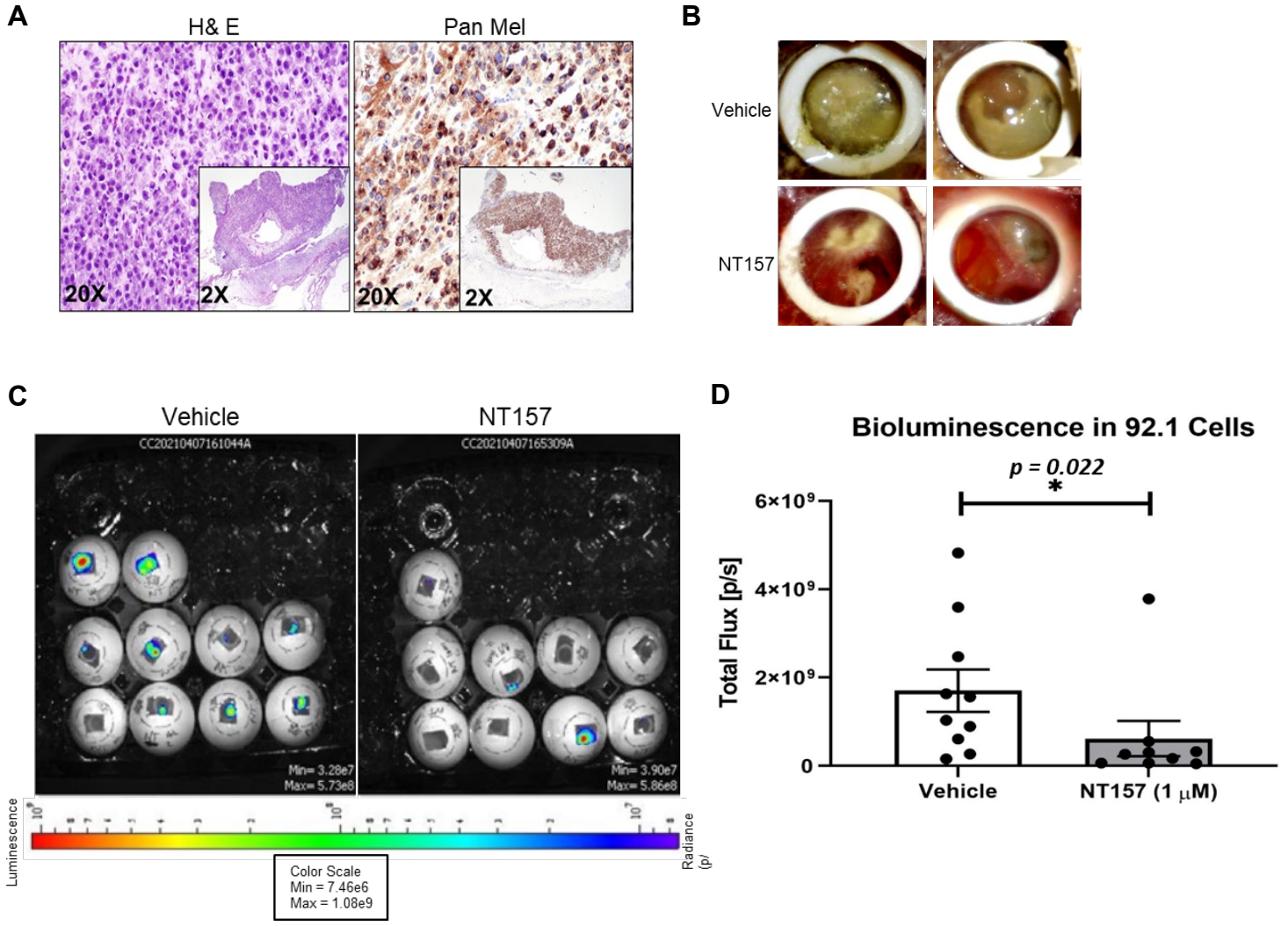
A
H& E
Pan Mel
20X
2X
20X
2X
B
Vehicle
NT157
C
Vehicle
NT157
CC20210407161044A
CC20210407165309A
Min= 3.28e7
Max= 5.73e8
Min= 3.90e7
Max= 5.86e8
Luminescence
Radiance
Color Scale
Min = 7.46e6
Max = 1.08e9
D
Bioluminescence in 92.1 Cells
p = 0.022
*
Total Flux [p/s]
6×10⁹
4×10⁹
2×10⁹
0
Vehicle
NT157 (1 μM)

Figure 5

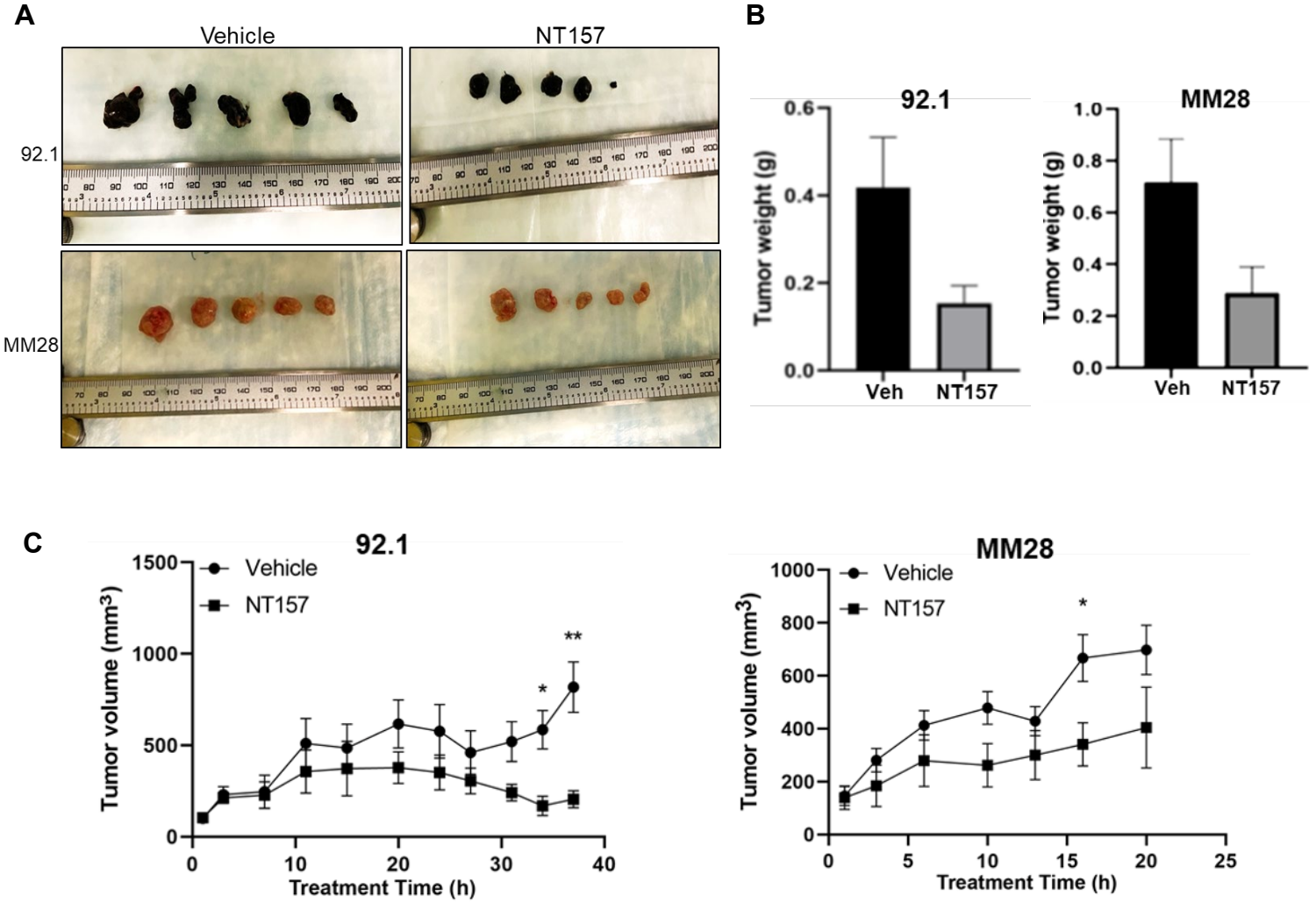
A
Vehicle
NT157
92.1
MM28
B
92.1
MM28
Tumor weight (g)
Veh
NT157
C
92.1
MM28
Vehicle
NT157
Tumor volume (mm3)
Treatment Time (h)
*
**

Supplemental Figure 1

A

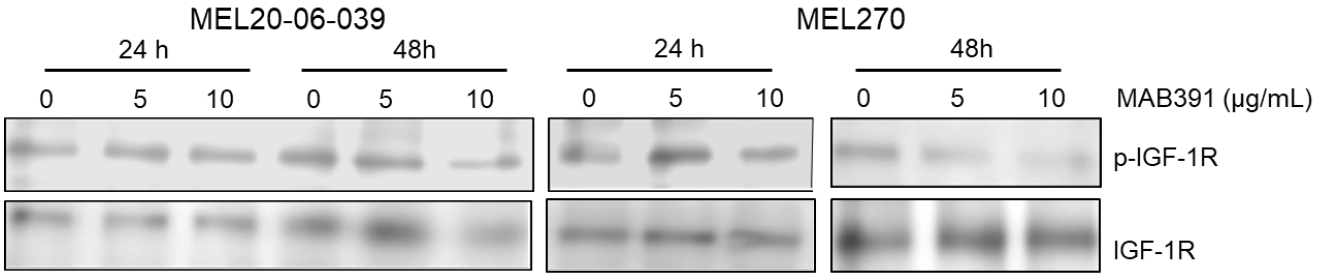

B

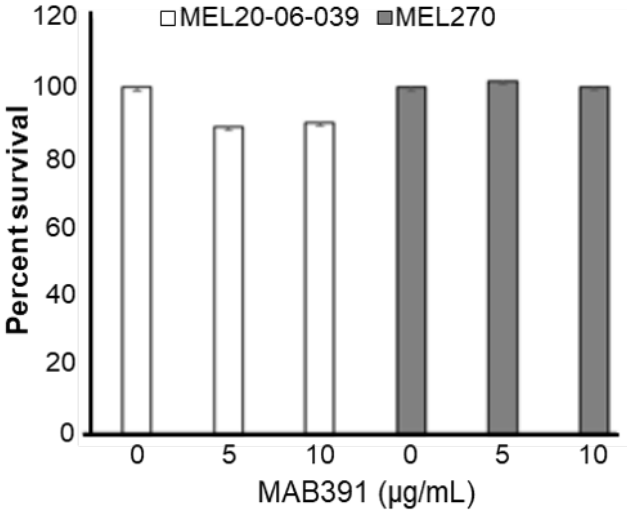

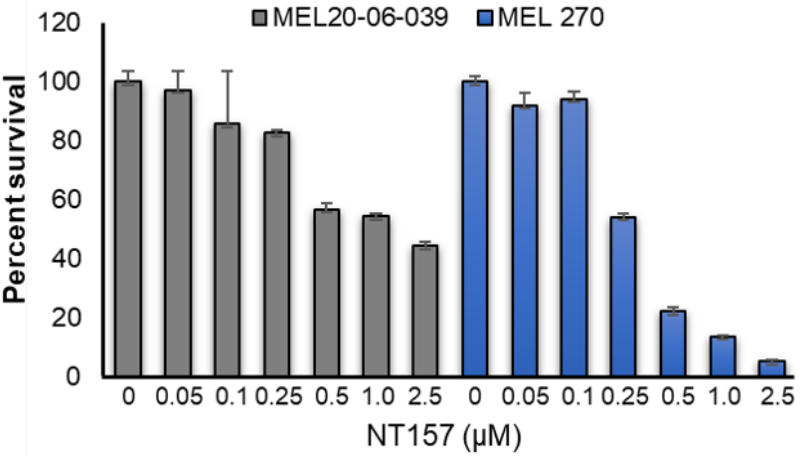

C

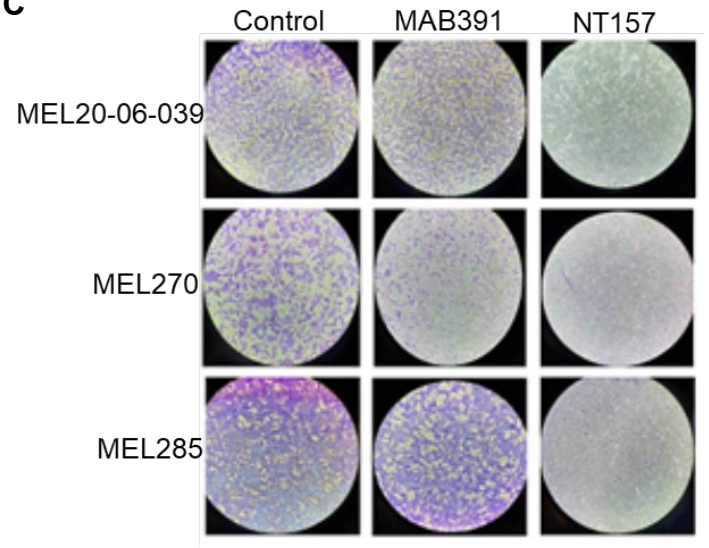

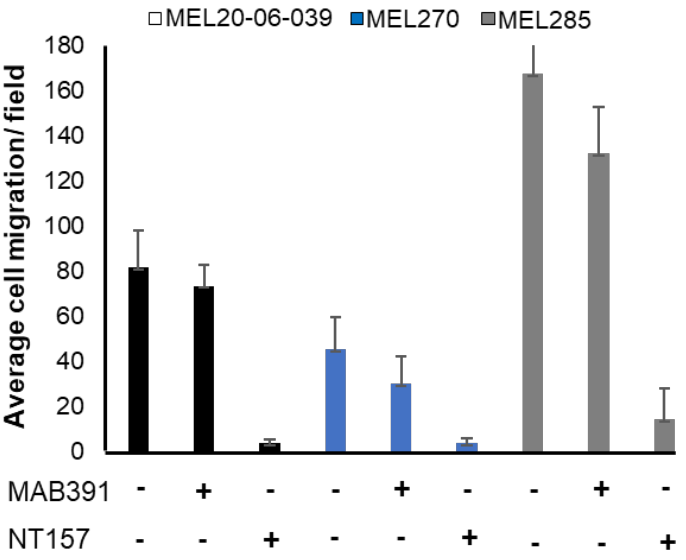
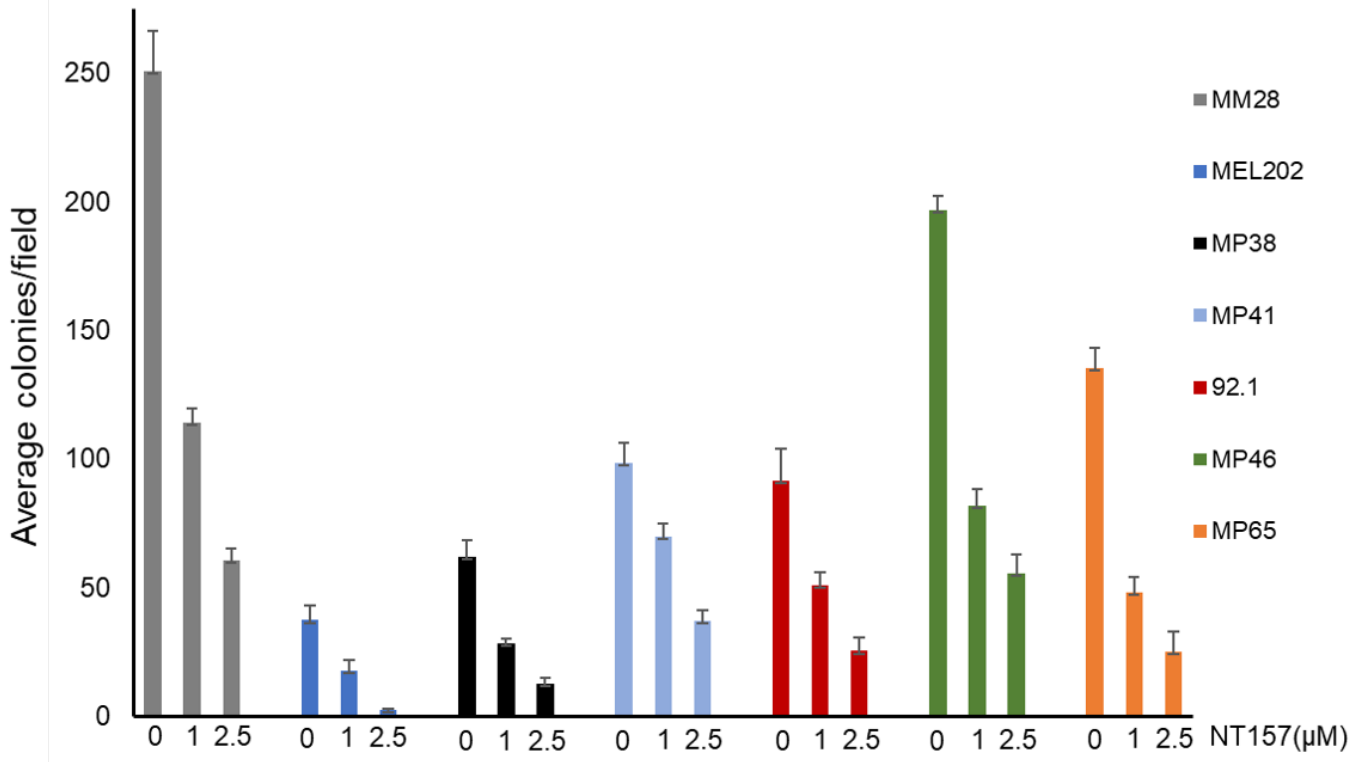
Supplemental Figure 2